Advanced Physics Research

ADVANCED PHYSICS RESEARCH

www.advphysicsres.com

RESEARCH ARTICLE OPEN ACCESS

Squeezed-Vacuum Bosonic Codes

Nir Gutman[1] | Eliya Blumenthal[2] | Shay Hacohen-Gourgy[2] | Ariel Orda[1] | Ido Kaminer[1]

[1]Viterbi Department of Electrical and Computer Engineering, Technion — Israel Institute of Technology, Haifa, Israel | [2]Department of Physics, Technion — Israel Institute of Technology, Haifa, Israel

Received: 6 April 2026 | **Accepted:** 8 April 2026

Keywords: bosonic codes | continuous variables | quantum error-correcting codes

ABSTRACT

We introduce a family of bosonic quantum error-correcting codes built as a rotation-symmetric superposition of squeezed vacuum states, which promise protection against both loss and dephasing noise channels. The robustness of these "squeezed-vacuum codes" arises from being arranged at evenly spaced angles in phase-space, and simultaneously in evenly spaced photon-number support $n \equiv 2k \pmod{2m}$. We present simple preparation circuits for general "m-legged" codewords using sequences of conditional rotations. The performance of these codes is evaluated against loss and dephasing noises using the Knill–Laflamme violation function and benchmarked against cat codes, binomial codes, and finite-energy GKP codes. As the number m of squeezed-vacuum states in a code increases, the code exhibits improved loss tolerance at the cost of higher dephasing sensitivity. We outline implementations in circuit QED and trapped-ion platforms, where high-fidelity Gaussian operations and conditional controls are available or under active development. These results help establish squeezed-vacuum codes as practical, hardware-compatible, members of the bosonic codes class.

1 | Introduction

Quantum computers promise exponential speed increases for certain computational tasks, but their fragile quantum states are extremely susceptible to noise. Quantum error-correcting codes (QECCs) [1, 2] protect logical quantum information by distributing it across a larger physical Hilbert space, enabling detection and correction of likely error processes. Topological codes, such as the surface code [3, 4], now dominate the road-maps of large-scale qubit processors, owing to their relative simplicity, yet at the cost of cumbersome logical operations [5] that require substantial qubit overhead.

An attractive alternative is to encode information in a bosonic mode, i.e., the infinite-dimensional Hilbert space of a single quantum harmonic oscillator. Because multiple indistinguishable excitations can occupy one resonator, bosonic codes can achieve the required redundancy while exploiting high-Q cavities for long coherence [6, 7]. These bosonic encodings naturally reside in the continuous-variable (CV) model of quantum computation, where quantum information is carried by the conjugate quadratures (q, p) of an oscillator. Lloyd et al. [8] proved that Gaussian operations — phase-space displacement $D(\alpha)$ and squeezing $S(r)$ — must be supplemented by at least one non-Gaussian element to achieve universal CV quantum computation.

Continuous-variable quantum error correcting-codes (CV-QECC) [9] leverages bosonic codes to protect against dominant noise channels, with landmark theoretical proposals including cat codes [10, 11], the Gottesman–Kitaev–Preskill (GKP) code [12], and finite-energy binomial codes [13]. Advances over the past two decades have gradually established a unified description of CV-QECC [14–16]. Such a general treatment enabled scientists to classify some encodings as part of the class of rotation-symmetric bosonic codes [17] with a generalized structure and gate set.

Experimental realizations of these codes have achieved significant milestones: Cat codes demonstrated break-even quantum error correction in superconducting cavities [18]. Binomial codes showed universal gate operations and error correction in superconducting cavities [19]. GKP codes were first realized on trapped-ion platforms [20] and demonstrated QEC with ∼3× longer logical coherences [21]; later implementations surpassed break-even and extended logical lifetimes to ∼2× that of their physical elements in superconducting circuits [22]; and were recently created on-chip in integrated photonics [23]. Different bosonic encodings are most naturally realized with different native non-Gaussian resources (e.g., conditional displacement or Kerr-type nonlinearities), whose implementation details and optimization are strongly platform-dependent. This motivates us to explore codes based on other non-Gaussian operations — specifically, conditional squeezing and conditional rotation — in order to offer alternative bosonic encodings built from distinct non-Gaussian primitives.

Here, we introduce a new family of bosonic error-correcting codes built from superpositions of vacuum states squeezed along evenly-spaced axes. The resulting codewords are simultaneously rotation-symmetric and also belong to the number-phase subclass [17] with sparse Fock support. The simplest 2-legged member achieves number code-distance 2 (i.e., loss events involving different numbers of photons map to disjoint subspaces) and an angular separation of $\pi/2$ between primitive squeezed states in phase-space, offering protection comparable to the 4-legged cat code. We find that a controlled-squeezing operation — squeezing the bosonic mode conditioned on a qubit's state [24–27] — can generate this 2-legged state in a single step. On top of this, we develop preparation protocols for all members of the code-family, based on conditional rotations and single qubit logic. We benchmark performance under photon loss and dephasing, comparing against cat codes. We then provide details on controlled squeezing across platforms and discuss implementation considerations.

The remainder of the paper is organized as follows: In Section 2, we introduce the squeezed-vacuum code family as a subclass of rotation-symmetric bosonic codes and describe its structure and distance properties. Next, Section 3 presents probabilistic and deterministic circuits for code preparation. Then, Section 4 discusses logical gates, state preparation, and readout for encoded qubits. Afterwards, Section 5 sets up loss and dephasing noise models and benchmarks the codes using a Knill–Laflamme cost, comparing against cat codes, binomial codes, and finite-energy GKP codes. Finally, Section 6 addresses the experimental feasibility (circuit QED and trapped-ion platforms) and provides guidelines for choosing code parameters; additional derivations and analysis appear in Appendices SA–SD of the Supporting Information.

2 | A New Family of Codes

2.1 | Motivation: Superpositions of Gaussian States as Bosonic Codes

Some of the simplest schemes that place Gaussian states in a superposition can protect against photon loss and dephasing [17]. A paradigmatic example is Schrödinger cat code, which stores a qubit in an m-legged superposition of coherent states [10, 11]. The legs are arranged equidistantly on a circle in phase space, endowing the state with an m-fold rotational symmetry that translates into resilience to particle-loss channels. Thus, by only manipulating Gaussian resources (displacements, squeezers, and phase shifters), one can control a rich highly-nonclassical code space. Our code family is such a surprisingly simple set.

Cat codes as a family. Rather than a single encoding scheme, cat states form a continuum parameterized by their mean photon number $|\alpha|^2$ and an integer m specifying the number of coherent-state "legs". Figure 3 depicts the familiar two-legged cat. Increasing m reduces the angular separation between the legs, thus improving particle-loss tolerance at the cost of less resilience to dephasing. This increased susceptibility to dephasing noise can be intuitively attributed to the larger number of states taking the same volume in phase-space (Figure 2).

2.2 | Required Operations

The canonical cat-code preparation uses a conditional displacement, in which an auxiliary qubit coherently displaces the oscillator to amplitudes $\pm\alpha$. We now build on this idea by replacing conditional displacement with conditional squeezing [25–27]. Both operations are non-Gaussian and share a similar structure. Making the conditional-squeezing operation explicit allows us to adapt the standard cat-code construction to obtain a new code family based on a different non-Gaussian primitive, and to systematically design and analyze circuits for preparing its codewords.

Recall the single-mode squeezing Hamiltonian [30]

$$H_S(\kappa) = \frac{i}{2}\left(\kappa\, a^{\dagger 2} - \kappa^*\, a^2\right), \tag{1}$$

whose conjugate coefficients ensure anti-Hermiticity of the generator. This Hamiltonian generates (for interaction duration t) a squeeze of magnitude $r = |\kappa| t$, corresponding to the unitary operator,

$$S(\zeta) = \exp\left[\frac{1}{2}\left(\zeta^* a^2 - \zeta\, a^{\dagger 2}\right)\right], \tag{2}$$

with $\zeta = re^{i\phi}$. Here, we would like to follow the notion of primitive-states in phase-space given in [17]. Our primitive state is a single squeezed-vacuum state [30], elongated along direction θ. We relate θ to ϕ with

$$\phi(\theta) = 2\theta + \pi \pmod{2\pi}, \tag{3}$$

which yields, e.g., $\theta = 0$ or $\theta = \pi \Rightarrow \phi = \pi$. We then define the direction-labeled squeezing unitary as

$$S(r, \theta) \equiv S\left(re^{i\phi(\theta)}\right). \tag{4}$$

Finally, we define the conditional squeezing unitary as

$$CS(r; \theta_0, \theta_1) = |0\rangle\langle 0| \otimes S(r, \theta_0) + |1\rangle\langle 1| \otimes S(r, \theta_1), \tag{5}$$

which applies squeezing that elongates vacuum along θ_0 (if the auxiliary qubit is $|0\rangle$) or along θ_1 (if it is $|1\rangle$). Proposals for implementation [24–27] of such an operation across multiple platforms (circuit QED, trapped ions) are discussed in Section 6.

2.3 | Squeezed-Vacuum Codes

Here we present a new family of Squeezed-vacuum codes defined by a coherent superposition of m differently oriented squeezing operations on the vacuum state. Each codeword is therefore a non-Gaussian superposition of Gaussian squeezed-vacuum states. For an even integer $m > 0$ and rotation-symmetry index $k \in [0, m-1]$ we set

$$|\psi_k\rangle \propto \sum_{j=0}^{m-1} e^{-i\frac{2\pi j}{m}k} S(r, \frac{\pi j}{m}) \, |\text{vacuum}\rangle \, . \tag{6}$$

In Fock space, this state occupies photon numbers $n \equiv 2k \pmod{2m}$, yielding natural logical codewords $|0_L\rangle := |\psi_0\rangle$ and $|1_L\rangle := |\psi_{m/2}\rangle$ whose number distributions are interleaved by $\Delta n = m$ (See Appendix SA for a derivation). Explicitly, $|0_L\rangle$ has nonzero Fock-state coefficients only at photon numbers $n = 0, 2m, 4m, \ldots,$ while $|1_L\rangle$ is supported on $n = m, 3m, 5m, \ldots$; notably, this occupancy pattern is independent of the squeezing strength r. The code distance is therefore d=m against single-photon loss events.

This sets the stage for the definition of a new family of single-mode bosonic error correction codes, as follows. For two parameters m and r — the even integer "number of legs" and the squeezing strength, correspondingly — two logical states are constructed from an equal (sometimes phased) superposition of squeezed states according to Equation (7):

$$\begin{aligned} |0_L\rangle &\propto \sum_{j=0}^{m-1} S(r, \frac{\pi j}{m}) \, |\text{vacuum}\rangle \, , \\ |1_L\rangle &\propto \sum_{j=0}^{m-1} (-1)^j \, S(r, \frac{\pi j}{m}) \, |\text{vacuum}\rangle \, , \end{aligned} \tag{7}$$

with a trivial normalization factor that keeps each state normalized to 1. Since single-primitive squeezed states are already limited to even Fock numbers, codes with an odd number of legs m are generally possible, but result in codewords without clear sparse Fock-number occupancy. Wigner functions resulting from this construction are depicted in Figure 2. A closed-form expression for the Fock-basis representation is derived in Appendix SA.

This family of codes — as a sub-family of rotation-symmetric bosonic codes — follows the same intuition from [17] that more primitives (more legs / larger m) results in a code that is more robust to loss but more susceptible to dephasing. We explore this notion numerically in Section 5. Additionally, this code is an "approximate number-phase code" [17] and we approach the "ideal number-phase code" at the limit of $r \to \infty$ (See discussion in Appendix SC).

3 | Preparation Circuits

In this section, we discuss probabilistic and deterministic methods for the generation of the bosonic codewords in the squeezed-vacuum family. We start with the simplest circuit, namely generating the code words for the 2-legged code, in a probabilistic manner. We then generalize to arbitrary even m-legged variants of the code. We also discuss the necessary operators needed to make these processes deterministic.

3.1 | 2-Legged Codewords

A minimal circuit to probabilistically prepare the m=2 codeword pair uses a Hadamard–Controlled-Squeezing–Hadamard (H–CS–H) sequence on a single auxiliary qubit coupled to a bosonic mode initially in the vacuum state; the probabilistic nature of this method arises from the final Z-basis measurement, collapsing the mode state to either an even or an odd superposition of squeezed states. Figure 3 illustrates that protocol and compares it to a similar sequence that generates the 2-legged cat code.

Although it might seem that the probability of getting either of the logical code states is equally distributed 50−50, this is not the case. Consider the case of r=0, equivalent to not performing squeezing at all. The logical-0 state reduces to the vacuum state, but the logical-1 state cannot be achieved. Therefore, we should expect a probability that scales somehow with the squeezing strength. In fact, the probability of getting the logical state L ($L \in \{0, 1\}$), given the squeezing strength r, is:

$$\text{prob}(L \mid r) = \frac{1}{2} + \frac{(-1)^L}{2\cosh r \sqrt{\tanh^2 r + 1}} \, . \tag{8}$$

As r increases, the probabilities approach a uniform distribution.

In most cases, such a probabilistic nature can be tolerated as long as we add post-selection on the measurement result.

3.2 | General m-Legged Codewords

Extending to m>2 by simply repeating the process in Section 3.1 would not work. Simply put, squeezing operations do not stack on top of each other: instead of creating more superpositions of primitive squeezed-vacuum states, more conditional-squeezings on top of states already squeezed would only rotate and stretch the existing states.

As shown in [24–26], controlled-squeezing promises universal control over the joint system of a qubit and a harmonic oscillator mode, once it is combined with displacement and (unconditional) squeezing on the mode and with full single-qubit control. In particular, the Lie-algebraic analysis of Ayyash et al. [24] demonstrates that including qubit-conditional squeezing generators in an already universal gate set enables more efficient synthesis of arbitrary unitaries on the joint Hilbert space, with accuracy that improves as the number of gates increases.

Two such unitaries that we can generate are: the conditional-rotation, $CR(\theta)$, which rotates the mode in phase space by θ if the state of the qubit (possibly in a superposition) is $|1\rangle$ (Equation 9); and the logical-X gate $\bar{X}$, which acts as the Pauli-X gate in the m-legged code-space, transforming the logical-0 state into a logical-1 state, and vice-versa (Equation 10).

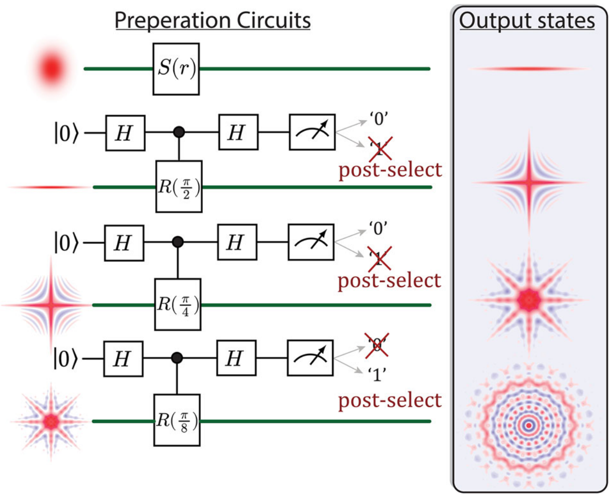

FIGURE 1 | Generation of multi-legged squeezed states: We present a new family of quantum error-correcting bosonic codes built from squeezed-vacuum states. Each codeword can be created by a sequence of single-qubit gates, conditional-rotations, and post-selection. Each resulted bosonic state can be fed back to generate a codeword with a larger superposition of squeezed-vacuum states. Selecting different measurement results generates different members of the family. In this example, the 8-legged logical-1 codeword is generated.

$CR(\theta)$ can be written as

$$CR(\theta) = |0\rangle\langle 0| \otimes \mathbb{1} + |1\rangle\langle 1| \otimes R(\theta), \tag{9}$$

where $R(\theta) = e^{i\theta a^\dagger a}$ rotates the state in phase-space by θ counter-clockwise. A discussion of experimental implementations and platform-dependent constraints is provided in Section 6.4.

$\bar{X}$ can be written as

$$\bar{X} = |0_L\rangle\langle 1_L| + |1_L\rangle\langle 0_L| + \mathbb{1}_\perp, \tag{10}$$

where $\mathbb{1}_\perp$ is the identity operator on the orthogonal complement of the code space. More on the implementation of $\bar{X}$ is discussed in Section 4.2. Note that as the squeezing strength r increases, the logical Pauli-X operation can be approximated by the operator $\sum_{n=0}^{\infty} |n\rangle\langle n+m|$, since the logical codewords approach "ideal number-phase codes" [17]. See related discussion in Appendix SC.

With these gates, we can establish the following algorithm for the generation of m-legged code states, for m=2^k with a positive-integer k. Starting with the qubit in $|0\rangle$ and the mode in $|\text{vacuum}\rangle$, we first squeeze our mode by r, creating the squeezed primitive state $S(r,0)\,|\text{vacuum}\rangle$. Then, we repeat the following sequence for $\log_2(m)$ iterations:

Apply $(H \otimes \mathbb{1})CR(\theta_j)(H \otimes \mathbb{1})$. At the j^{th} iteration, $\theta_j = \frac{\pi}{2^j}$. Then, measure the qubit. If this is the last iteration, the result of the measurement dictates whether we are in the logical-0 or logical-1 state. Otherwise, only the $'0'$ result should be kept for the next iterations. One can either use post-selection (probabilistic) or a feed-forward conditional X_L correction (deterministic) to keep the desired result. This algorithm is summarized in Algorithm 1 and visually exemplified in Figure 1.

ALGORITHM 1 | Preparation of 2^k-legged codewords using conditional-rotations

Inputs: r, k, $\hat{L}$ ▷ $\hat{L} \in \{0,1\}$ is the desired codeword
Initialize bosonic mode in $|\text{vacuum}\rangle$
$|\text{mode}\rangle \leftarrow S(r,0)\,|\text{vacuum}\rangle$ ▷ Apply squeezing
for $j = 1$ to k **do**
  $\theta_j \leftarrow \frac{\pi}{2^j}$
  $|\psi\rangle = |0\rangle \otimes |\text{mode}\rangle$ ▷ Initialize qubit in $|0\rangle$
  $|\psi\rangle \leftarrow (H \otimes \mathbb{1})\,CR(\theta_j)\,(H \otimes \mathbb{1})\,|\psi\rangle$
  Measure the qubit in the Z basis
  $L \leftarrow$ measurement result ▷ $L \in \{0,1\}$
  $|\text{mode}\rangle \leftarrow |\psi\rangle$ traceover qubit
  ▷ deterministic or probabilistic part (see Note):
  if $j < k$ **then**
    continue only if $L = 0$
  else
    return $|\text{mode}\rangle$ if $L = \hat{L}$
  end if
end for

Note: If an undesired outcome L occurs, two approaches are possible. In a deterministic protocol, one applies a corrective logical-X operation (Equation 10) on $|\text{mode}\rangle$. In a probabilistic protocol, one instead uses post-selection, i.e., discards the current run and repeats until the desired outcome is obtained.

This rather simple protocol can generate only codewords of the m=2^k-legged variants. To generate a general even m-legged state, we apply a single iteration of the previous protocol on an already $\frac{m}{2}$-legged state in an equal superposition $|e_{\frac{m}{2}}\rangle = \sum_{j=0}^{\frac{m}{2}-1} S(r, \frac{2\pi j}{m})\,|0\rangle$. If $\frac{m}{2} = 2^k$ for some k, then we can use the protocol from Algorithm 1, accepting only the logical-0 codeword (which is of an equal superposition as required); Otherwise, $|e_{\frac{m}{2}}\rangle$ can be achieved with another protocol, summarized in Algorithm 2. For this protocol, we will introduce an operation that conditionally applies a rotation with phase, which we will write as $CR_{\text{phased}}(\theta, \phi)$ (Equation 11).

$$CR_{\text{phased}}(\theta, \phi) = |0\rangle\langle 0| \otimes \mathbb{1} + e^{i\phi}\,|1\rangle\langle 1| \otimes R(\theta). \tag{11}$$

This operation can be decomposed as a conditional rotation preceded by a phase gate on the qubit:

$$CR_{\text{phased}}(\theta, \phi) = \left(e^{i\phi|1\rangle\langle 1|} \otimes \mathbb{1}\right) CR(\theta), \tag{12}$$

where the phase gate $e^{i\phi|1\rangle\langle 1|} = |0\rangle\langle 0| + e^{i\phi}\,|1\rangle\langle 1|$ acts only on the qubit.

Both Algorithms 1 and 2 share a common recursive structure and admit two implementation approaches: a purely probabilistic protocol that relies on post-selection of measurement outcomes, or a deterministic protocol that applies feed-forward $\bar{X}$ corrections based on the measurement results. However, the implementation

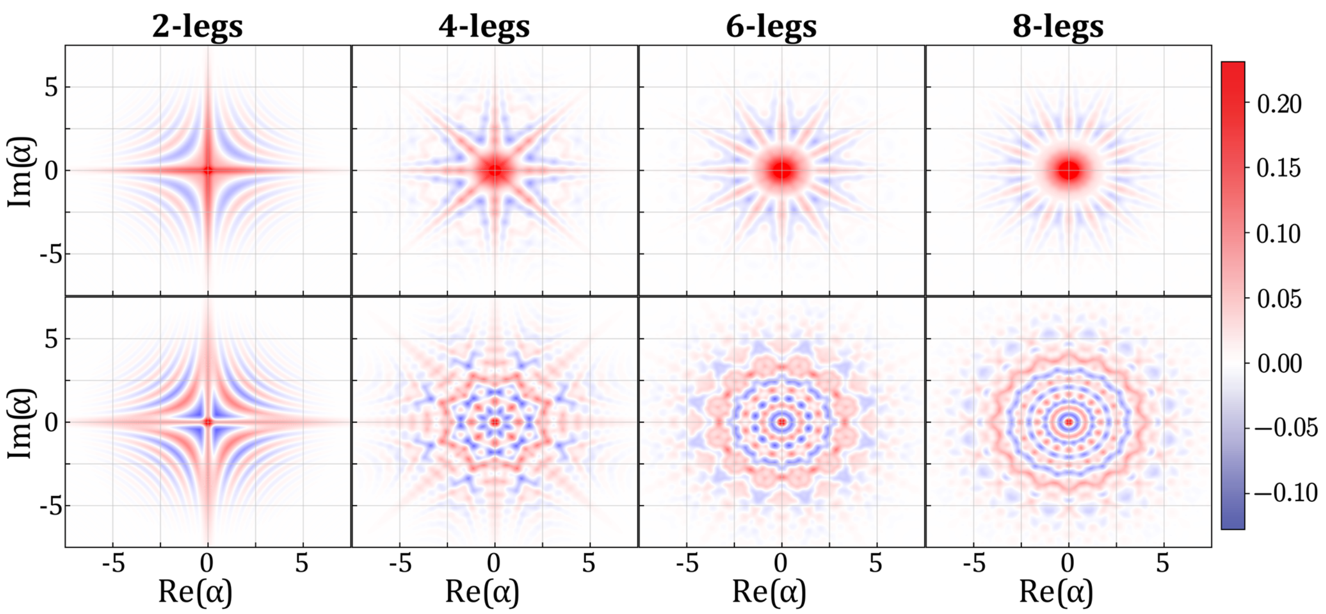

FIGURE 2 | The family of multi-legged squeezed bosonic codes: Wigner functions [28] of m-legged squeezed codes for $m=2\dots8$ at fixed squeezing strength $r=1.5$. For each m, we show 2 logical codewords. Increasing the number of legs increases m-fold rotation symmetry and protection against particle loss. The upper-left Wigner function was previously shown [29] but had not been analyzed there as a bosonic code.

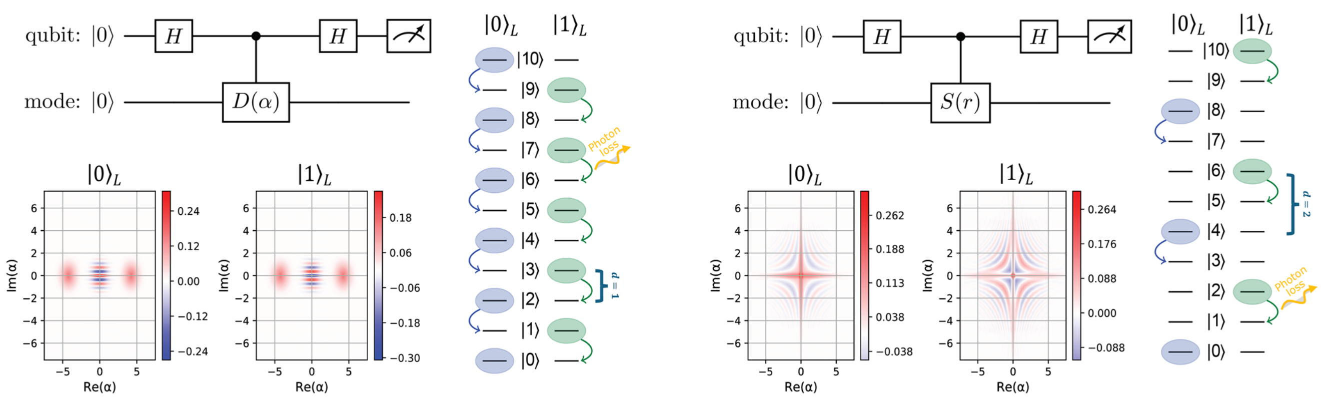

FIGURE 3 | Generating scheme of multi-legged squeezed codes vs cat codes: Comparing a conventional circuit for generating the 2-legged Schrödinger's cat state [31] using a conditional-displacement gate $CD(\alpha)$ (a1) and our 2-legged squeezed code using a conditional-squeezing gate $CS(r;0,\frac{\pi}{2})$ Equation 5 (b1). Wigner functions [28] of the resultant states are shown in (a2,b2). The support of the codes in Fock space is also compared (a3,b3): While the 2-legged cat code has a number distance of d=1 (a3) with respect to photon loss events, our code has a number distance of d=2, meaning that single-photon loss events map to disjoint subspaces (b3). The number distance increases linearly for both codes as the number of legs m increases. Circuits drawn with [32].

of $\bar{X}$ is non-trivial (as discussed in Section 4.2), making the purely probabilistic approach more suitable in most cases. In Figure 4, we analyze the probability of successfully generating the different logical states at the end of these protocols for various numbers of legs m.

Python implementations of these protocols can be found in our code [33].

4 | Logical Operations

Having defined the squeezed-vacuum codewords, we now turn to the question of universal quantum computation. In this section, we suggest ways to achieve universal control over the encoded qubits by distinguishing between "native" gates—those realized by simple physical Hamiltonians—and operations that require gate teleportation. We show that the rotation symmetry of our codes gives immediate access to a logical $\bar{Z}$ and a logical $\overline{\text{CZ}}$. We then describe how to complete the universal set using teleportation, discuss strategies for state preparation, and outline measurement primitives.

The codewords in Equation 7 have support only on photon numbers $n=(2k+\ell)m$, corresponding to an order-m rotation-symmetric code [17]. Consequently, the general logical toolbox developed for number–phase codes applies directly to our family. Accordingly, most of this section follows the established number-phase-code framework of Ref. [17].

ALGORITHM 2 | Preparation of m-legged squeezed states in equal superposition using conditional rotations

Inputs: $r,\ m$
Initialize bosonic mode in $|\text{vacuum}\rangle$
$|\text{mode}\rangle \leftarrow S(r,0)\,|\text{vacuum}\rangle$ ▷ Apply squeezing
$\theta \leftarrow \frac{2\pi}{m}$
for $j = 1$ to $m-1$ **do**
  $\phi_j \leftarrow \pi - \frac{2\pi j}{m}$
  $|\psi\rangle = |0\rangle \otimes |\text{mode}\rangle$ ▷ Initialize qubit in $|0\rangle$
  $|\psi\rangle \leftarrow (H \otimes \mathbb{1})\, CR_{\text{phased}}(\theta, \phi_j)\, (H \otimes \mathbb{1})\, |\psi\rangle$
  Measure the qubit in the Z basis
  $L \leftarrow$ measurement result ▷ $L \in \{0, 1\}$
  $|\text{mode}\rangle \leftarrow |\psi\rangle$ traceover qubit
  ▷ deterministic or probabilistic part (see Note):
  continue only if $L = 0$
end for
return $|\text{mode}\rangle$

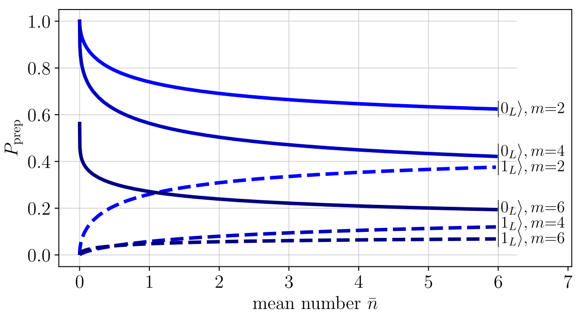

FIGURE 4 | Probability of successfully generating logical states. Probability of successfully generating the different logical states at the end of the protocols in Algorithms 1 and 2 for various numbers of legs m. The probabilities are plotted as a function of the mean (photon) number $\bar{n}$, which depends on the squeezing strength r as shown in Equation S(25) in Appendix SA.

4.1 | Native Gates: $\bar{Z}$ and $\overline{\text{CZ}}$

The rotation symmetry of the code allows us to implement diagonal Clifford gates using simple physical interactions.

Logical $\bar{Z}$ The logical Pauli-Z is implemented by a phase-space rotation:

$$\bar{Z} = R\left(\frac{\pi}{m}\right) = \exp\left(i\frac{\pi}{m}a^\dagger a\right). \tag{13}$$

This operator acts as the identity on the logical $|0_L\rangle$ (supported on even multiples of m) and applies a (-1) phase to the logical $|1_L\rangle$ (supported on odd multiples of m).

Entangling gate $\overline{\text{CZ}}$ Universal computation requires entanglement between bosonic modes. We leverage a controllable cross-Kerr interaction $H_{\text{int}} \propto a^\dagger a \otimes b^\dagger b$, which has become viable across multiple platforms including cQED and trapped ions [34–36]. For two encoded modes a and b with parameters m_a and m_b, the logical entangling gate is:

$$\overline{\text{CZ}} = \exp\left(i\frac{\pi}{m_a m_b}\, a^\dagger a \otimes b^\dagger b\right), \tag{14}$$

which acts as a logical controlled-Z on the encoded subspace. Indeed, for Fock states in the code support, $n_a = (2k + \ell_a)m_a$ and $n_b = (2k' + \ell_b)m_b$ with $\ell_a, \ell_b \in \{0, 1\}$, $e^{i\frac{\pi}{m_a m_b} n_a n_b}\,|n_a, n_b\rangle = e^{i\pi(2k+\ell_a)(2k'+\ell_b)}\,|n_a, n_b\rangle = (-1)^{\ell_a \ell_b}\,|n_a, n_b\rangle$ which is exactly a $\overline{\text{CZ}} = \text{diag}(1, 1, 1, -1)$ on the logical basis.

4.2 | Completing the Universal Set

While the diagonal gates $\bar{Z}$ and $\overline{\text{CZ}}$ are native, the code lacks a simple unitary for the logical $\bar{X}$ or $\bar{H}$. To achieve universality, we rely on gate teleportation utilizing the $\overline{\text{CZ}}$ interaction derived above [17].

Specifically, the logical Hadamard $\bar{H}$ is implemented by coupling the data mode to a logical auxiliary mode prepared in $|+_L\rangle$ via a $\overline{\text{CZ}}$ gate, followed by a measurement of the data mode in the logical X basis (see Section 4.4). Crucially, this scheme does not require a physical $\bar{X}$ gate. Any Pauli-$\bar{X}$ corrections arising from the teleportation measurement outcome are tracked in the Pauli frame (software tracking), meaning subsequent operations are classically updated rather than applying a physical recovery pulse. Non-Clifford gates, such as the logical $\bar{T}$, are implemented similarly by injecting magic states prepared in a physical auxiliary qubit.

4.3 | Preparing Arbitrary States

The ability to initialize the code in an arbitrary superposition $|\psi_L\rangle = \alpha\,|0_L\rangle + \beta\,|1_L\rangle$ is essential for computation. In contrast to the preceding material, this subsection introduces a rotated-measurement-frame preparation variant that is not presented in Ref. [17].

Standard protocols for state preparation rely on *injection*: preparing the target state on a physical auxiliary qubit and teleporting it into the code via the gate mechanisms described in Section 4.2 [17]. While generic, this approach requires an additional logical auxiliary mode and inter-mode entangling gates.

Here, we highlight an alternative method that synthesizes arbitrary states directly during the initialization protocol described in Section 3.2. This method absorbs the target coefficients α, β into the measurement basis of the final step of the preparation circuit. The basis-adapted single-qubit measurement used in this final step follows the measurement-based preparation paradigm introduced in one-way quantum computation [37]. Specifically, we insert a single-qubit rotation $U_{\text{rot}}(\theta, \varphi) = R_y(-\theta)\,R_z(\varphi)$ on the physical auxiliary qubit immediately before the final measurement (Figure 5), where θ and φ are the Bloch-sphere polar and azimuthal angles of the target state, respectively; such that $\alpha = \cos(\theta/2)$ and $\beta = e^{i\varphi}\sin(\theta/2)$. This rotation maps the target superposition to the measurement axis, such that outcome ‘0’ projects the bosonic mode onto $|\psi_L\rangle$.

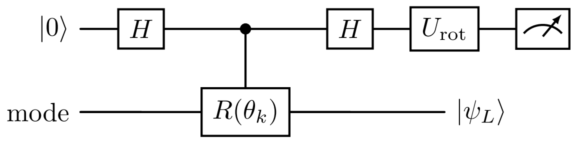

FIGURE 5 | Rotated-measurement-frame circuit. Final iteration of the preparation protocol with the single-qubit rotation $U_{\mathrm{rot}}(\theta, \varphi) = R_y(-\theta)\, R_z(\varphi)$ inserted before measurement. The outcome '0' yields $|\psi_L\rangle = \alpha\,|0_L\rangle + \beta\,|1_L\rangle$; outcome '1' yields its orthogonal complement.

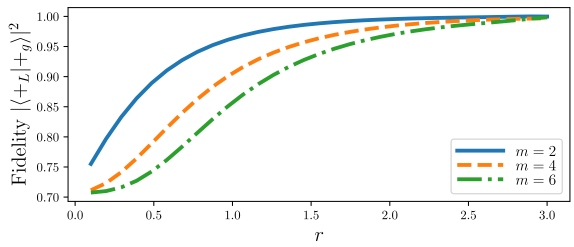

FIGURE 6 | Fidelity of the rotated-measurement-frame preparation. Fidelity $|\langle +_L|+_g\rangle|^2$ between the ideal logical $|+_L\rangle$ and the state $|+_g\rangle$ produced by the rotated-frame circuit, as a function of the squeezing parameter r, for $m = 2, 4, 6$.

This approach avoids the need for a separate logical auxiliary mode $|+_L\rangle$ or a difficult logical $\bar{X}$ gate. However, this is not an exact state-preparation scheme: the physical mode state produced by the circuit only approximates the ideal encoded target. This discrepancy arises because the codeword normalization constants $\mathcal{N}_\ell$ differ at finite energy (see Equation S(24) in Appendix SA), becoming equal only in the limit of large squeezing r. Consequently, the infidelity is not uniform across the code space but scales with two factors: (i) the distance of the target state from the computational basis states $|0_L\rangle$ or $|1_L\rangle$ on the logical Bloch sphere (where the normalization mismatch is most pronounced), and (ii) the magnitude of the squeezing parameter r (i.e., how far the code is from the ideal number-phase limit). Figure 6 quantifies this effect, comparing the fidelity of the state $|+_g\rangle$ generated by this method with the ideal $|+_L\rangle$ as a function of r.

4.4 | Logical Readout

To complete the computational cycle, we require measurements in the logical Pauli bases.

4.4.1 | Logical Z (Photon Number)

Since the codewords $|0_L\rangle$ and $|1_L\rangle$ have disjoint support on the number lattice (even vs odd multiples of m), a logical $\bar{Z}$ measurement corresponds to measuring the photon number modulo $2m$. This can be performed destructively via photon counting, or non-destructively by mapping the number parity to an auxiliary qubit.

4.4.2 | Logical X (Phase)

Measurements in the logical $\bar{X}$ basis correspond to distinguishing the dual codewords $|\pm_L\rangle$. These codewords lie in distinct sectors of phase space, such that distinguishing them requires only coarse-grained phase estimation. Resolving the phase of the oscillator modulo $2\pi/m$ distinguishes between the constructive and destructive interference patterns of the superposition states. In practice, this is implemented via heterodyne or adaptive-homodyne detection, where the continuous measurement record is digitized to the nearest sector on the phase lattice [38].

5 | Numerical Analysis

Errors in quantum systems are modeled by completely positive and trace-preserving (CPTP) linear maps (quantum channels). One convenient description is a channel's Kraus (operator-sum) representation:

$$\mathcal{N}_\gamma(\rho) = \sum_j K_j\, \rho\, K_j^\dagger, \quad \sum_j K_j^\dagger K_j = \mathbb{1}. \tag{15}$$

This representation is not unique.

In applications related to quantum computation with bosonic codes, the dominant noise processes are loss [1] and dephasing, each with its infinite series of Kraus operators, given here as a function of a noise-strength γ [39]:

$$\begin{aligned} K_j^{\mathrm{loss}}(\gamma) &= \sqrt{\frac{\gamma^j}{j!}}\,(1-\gamma)^{\frac{n}{2}}\, a^j, \\ K_j^{\mathrm{dephasing}}(\gamma) &= \sqrt{\frac{\gamma^j}{j!}}\, e^{-\frac{\gamma}{2}n^2}\, n^j, \end{aligned} \tag{16}$$

where γ is the unitless noise-strength coefficients, a is the annihilation operator and $n = a^\dagger a$. These two error channels commute [39, 40], thus allowing independent analysis.

The performance of a bosonic code with two orthonormal logical codewords $|0_L\rangle$ and $|1_L\rangle$ can be measured according to its Knill–Laflamme (KL) violation. The original KL conditions for exact correctability are $\langle i_L|K_a^\dagger K_b|j_L\rangle \propto \delta_{ij}$ [41]. Exact satisfaction of these conditions yields a perfect code with

$$\begin{aligned} \langle 0_L|K_a^\dagger K_b|0_L\rangle &= \langle 1_L|K_a^\dagger K_b|1_L\rangle = 1 \quad \forall a, b\,, \\ \langle 0_L|K_a^\dagger K_b|1_L\rangle &= \langle 1_L|K_a^\dagger K_b|0_L\rangle = 0 \quad \forall a, b\,. \end{aligned} \tag{17}$$

Approximately satisfying them gives rise to realistic, experimentally accessible codes that correct errors only up to a given tolerance.

One way to measure the performance of an approximate code is to sum the deviation from Equation (17) for specific bra $\langle i|$ and ket $|j\rangle$, along all Kraus operators in a given noise-channel. We call this the KL-violation of $\langle i|$ and $|j\rangle$ over noise-channel $\mathcal{N}$. An exact formula is given in Equation (18):

$$V_{\mathrm{KL}}(\mathcal{N})_{i,j} = \sum_{a,b} \left| \delta_{ij} + (-1)^{\delta_{ij}} \langle i|\, K_a^\dagger K_b\, |j\rangle \right|. \tag{18}$$

Summing over all Kraus operators in an infinite series (Equation 16) is impossible in numerical analysis, so a cut-off must be

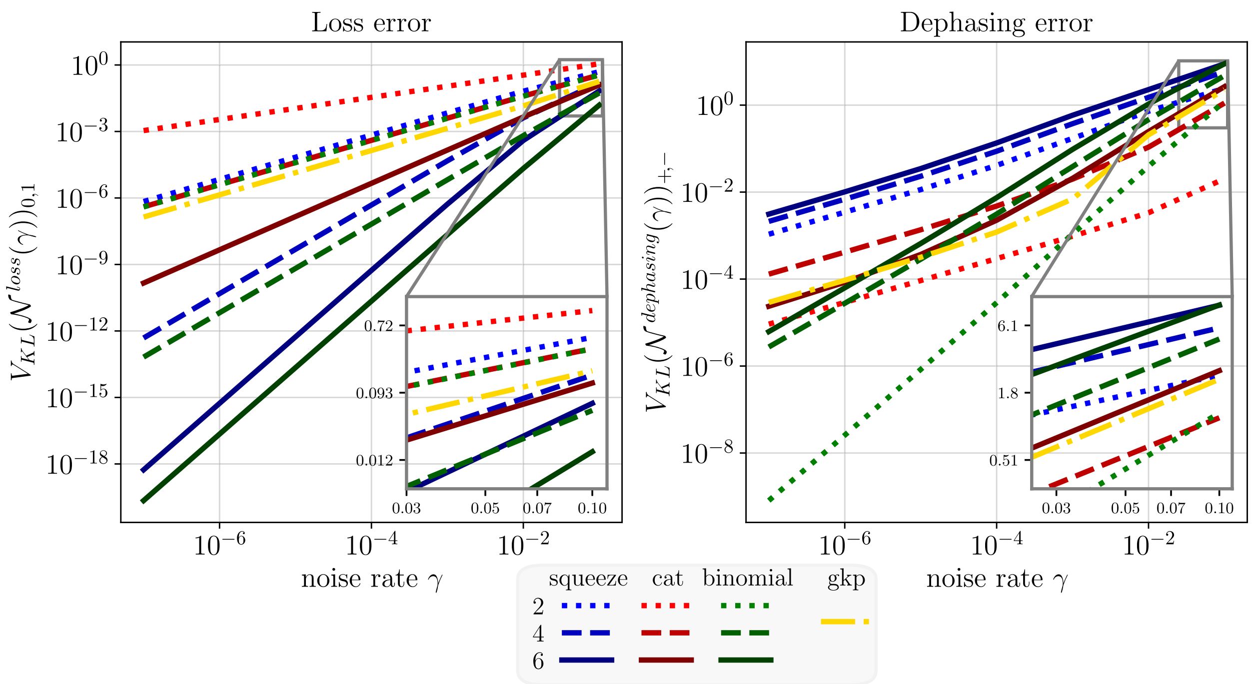

FIGURE 7 | Error correction as noise increases: Plotting $V_{\mathrm{KL}}(\mathcal{N})_{0,1}$ (Equation 18) for loss noise and $V_{\mathrm{KL}}(\mathcal{N})_{+,-}$ for dephasing noise, over strengths γ. Exact KL conditions satisfactions occurs at $V_{\mathrm{KL}}(\mathcal{N}) = 0$ hence smaller values indicate better code performance. We compare our squeezed-vacuum codes to the established cat codes and binomial codes each with "number-of-legs" 2, 4, and 6, and to the square GKP code. In the legend, the row labels 2, 4, and 6 denote the number of legs for the squeezed-vacuum, cat, and binomial families. Here, the code parameters are chosen so that all codes are compared with the same mean (photon) number $\bar{n}$=3 for $|0_L\rangle$ (See Equation S(25) in Appendix SA). One can observe that increasing the number of legs protects against loss better at the cost of worse protection against dephasing. The insets highlight the high-error regions ($\gamma \in [0.03, 0.10]$) to clarify the performance crossovers.

chosen. Choosing a cut-off in a way that keeps the results accurate up to a predetermined tolerance is discussed in Appendix SB.

Additionally, the Knill–Laflamme violation strictly assumes an exactly orthonormal basis. For finite-energy codes such as the square GKP code, the physical codewords exhibit a slight inherent non-orthogonality. To accurately evaluate the dynamics without introducing a static baseline error, we apply symmetric (Löwdin) orthogonalization [42] to strictly define the logical code space prior to the calculation (see Appendix SB for details).

It is also possible to sum $V_{\mathrm{KL}}(\mathcal{N})_{i,j}$ over all logical i, j states combinations — into a single "KL cost function" [43]. This allows computerized optimization protocols to choose a specific code scheme for a given system under constraints and other considerations. Even more methods to compare the performance of single-mode bosonic codes are emerging. For example, methods that take the recovery procedure into account [16, 44]. There is a plethora of other options that we will not discuss in this paper.

Figure 7 shows $V_{\mathrm{KL}}(\mathcal{N})_{0,1}$ for loss noise and $V_{\mathrm{KL}}(\mathcal{N})_{+,-}$ for dephasing noise, each over different noise-strengths γ. The dual codewords $\left\{ |+_L\rangle = \frac{1}{\sqrt{2}}(|0_L\rangle + |1_L\rangle),\ |-_L\rangle = \frac{1}{\sqrt{2}}(|0_L\rangle - |1_L\rangle) \right\}$ are more prone to dephasing error, so it is more fair to test code performance given those states. Examining the high-noise regimes shown in the insets reveals distinct behaviors. In the loss channel (left), all codes ultimately degrade to a similarly poor level of performance, reflecting a general breakdown of correctability. In the dephasing channel (right), however, a notable crossing occurs: while the 2-leg binomial code provides the best error suppression at low noise, its performance decays much faster than its peers as noise increases. At high dephasing noise, it is surpassed by the simpler 2-legged cat code, which exhibits a lower absolute Knill–Laflamme violation in this extreme regime.

Figure 8 shows $V_{\mathrm{KL}}(\mathcal{N})_{0,1}$ the same KL-violation analysis but at a fixed noise-strength γ=10^{-4} and different mean (photon) numbers $\bar{n}$. The results demonstrate that for most codes, increasing the mean number $\bar{n}$ leads to higher error rates. In the loss channel (left), the error for squeezed-vacuum and cat codes rises with $\bar{n}$ because the effective interaction with the environment scales with the number of excitations. The dephasing channel (right) shows a similar penalty, as the noise is driven by the n^2 term in the Kraus operators, which disproportionately affects states with higher energy. While binomial codes show specific points of resiliency due to their design, the general trend indicates that without active correction, larger states are intrinsically more vulnerable to environment-induced overlap. For completeness, a supplementary evaluation at a higher fixed noise of γ=10^{-2} is provided in Appendix SD (see Figure 9).

It is important to emphasize that the KL-violation benchmark used here is recovery-agnostic; it measures the intrinsic compatibility between the code and the noise channel rather than the end-to-end performance of an optimized active correction protocol. Consequently, we do not claim universal superiority of squeezed-vacuum codes over established codes for which

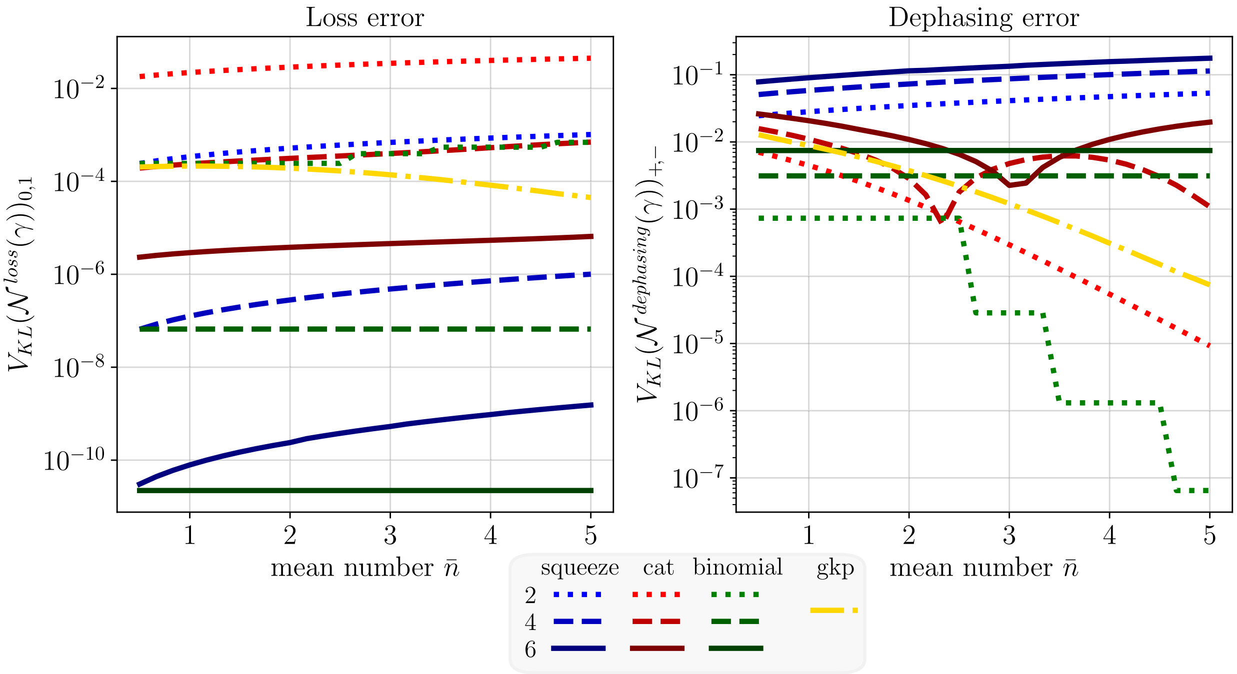

FIGURE 8 | Error correction as mean number increases: We compare our squeezed-vacuum codes to the established cat codes, binomial codes and the square GKP code. In the legend, the row labels 2, 4, and 6 denote the number of legs for the squeezed-vacuum, cat, and binomial families. Here the noise-strength is fixed at $\gamma=10^{-4}$ and Equation 18 is plotted for different mean number $\bar{n}$ for $|0_L\rangle$ (See Equation S(25) in Appendix SA).

practical stabilization or active correction sequences already exist. Instead, the results highlight a fundamental trade-off: increasing the number of legs improves robustness against loss while reducing robustness against dephasing. The optimal choice of code is thus heavily dependent on the specific physical platform and available control capabilities. Accordingly, the present manuscript does not attempt a recovery-dependent operational benchmark; rather, it focuses on KL-based intrinsic code-channel compatibility, while explicit recovery-map performance is left for future work.

Finally, performance comparisons as a function of the mean photon number $\bar{n}$ should be viewed together with the effort required to prepare the corresponding logical states. When the preparation is run in the purely probabilistic (post-selection) mode of Algorithms 1 and 2, the success probability depends on r. As shown in Figure 4, for small mean number $\bar{n}$ the post-selected preparation of the $\ell=1$ (logical $|1_L\rangle$) state can be significantly less likely than that of $|0_L\rangle$, so generating $|1_L\rangle$ may require more repeated attempts even though the resulting low-energy codewords can perform well once available. This preparation aspect should be considered when choosing the optimal code parameters for a given platform.

Our numerical analysis can be replicated through our (freely-accessible) code [33].

6 | Discussion and Outlook

The practical realization of bosonic codes relies on matching the code structure to the native operations available on a given hardware platform. Standard encodings often utilize conditional displacements and Kerr-type nonlinearities, which have achieved impressive fidelities in recent experiments. For instance, high-fidelity conditional displacements are readily available in circuit QED as echoed conditional displacements [45] — a promising enabler for break-even quantum error correction [22] — and manifest as native spin-dependent forces in trapped ions [46], enabling deterministic grid state preparation, as proposed in Ref.[47] and realized in Ref.[21]. Similarly, Kerr nonlinearity is a native resource in superconducting circuits and is being explored in trapped-ion systems via proposals utilizing tweezer potentials [48] or operation outside the Lamb-Dicke regime [49, 50].

However, synthesizing complex code states purely from these elementary primitives often requires an impractical amount of resources; for example, realizing effective Kerr nonlinearity from conditional displacements requires deep gate sequences [51]. Consequently, the field is rapidly advancing toward utilizing specialized, higher-order nonlinearities to facilitate large-scale encodings [52, 53], exemplified by theoretical proposals such as Tiger codes [54] and recent experimental demonstrations [55, 56]. Our proposed squeezed-vacuum codes align with this trend by relying on a distinct set of primitives—specifically conditional squeezing and conditional rotation—which we now discuss in the context of specific experimental platforms.

6.1 | Circuit-QED Platform Readiness

Practical deployment of the squeezed-vacuum code depends on the availability of high-fidelity Gaussian operations (displacements, rotations, squeezing) together with conditional control. Circuit QED platforms are particularly promising: universal oscillator control via a weakly-dispersive auxiliary qubit has been established and scaled to fast, high-fidelity gates [45, 57]. In this toolbox, number-selective conditional rotations (SNAP-type gates) [58], and high-quality single-mode squeezing has been demonstrated [45]. However, a modular, high-fidelity qubit-conditional squeezing gate is not yet a routine experimental primitive in cQED. Several concrete proposals exist in standard transmon–cavity hardware [24–26], but (to our knowledge) gate-level experimental benchmarks are still missing.

6.2 | Trapped Ions Platform Readiness

Trapped-ion systems have demonstrated comparable levels of squeezing and even deterministic preparation of GKP logical states in the motional modes of a single ion [20, 59]. With access to sideband couplings (spin-dependent forces) [60], and optimal-control pulse shaping for spin–motion dynamics [59], trapped-ion platforms can realize conditional Gaussian primitives, including state-dependent displacement [60] and controlled-squeezing [61, 62]. These, together with a recent high-fidelity demonstration of strong spin-dependent squeezing of a near-ground-state motional mode [63], place trapped-ions on the path towards implementing the suggested code family.

At the level of control primitives, trapped-ion platforms routinely engineer conditional Gaussian operations on motion using bichromatic near-sideband driving (spin-dependent forces); see Leibfried et al. [64] for a review. Beyond single-ion state engineering, spin-dependent squeezing has been leveraged in trapped-ion gate design, including proposals for programmable many-body interactions [65] and robustness-enhanced two-qubit entangling gates [66], and has been incorporated into larger experimental gate sequences [67]. Because these approaches typically rely on higher-order sideband couplings, the effective squeezing interaction can be intrinsically weaker (hence slower) in the Lamb–Dicke regime and may incur additional power/time overheads [65, 66].

6.3 | Creation of Controlled-Squeezing

Recent proposals and demonstrations across platforms indicate growing readiness for the implementation of a controlled-squeezing operation (Equation 5). In circuit QED, Blumenthal et al. [26] propose using a Rabi-driven qubit dispersively coupled to one or two high-Q oscillators to implement conditional single- and two-mode squeezing entirely within the cavity, predicting up to ~ 4 dB of single-mode squeezing in superposition and estimating qubit-oscillator entanglement without additional nonlinear elements. Independently, Del Grosso et al. [25] introduce a controlled-squeeze gate in a resonator terminated by a SQUID (superconducting quantum interference device) that applies $S(r,\theta)$ when the qubit is in $|1\rangle$. In related theoretical work, Ayyash et al. [24] develop a general theory of drive-enhanced multiphoton qubit–resonator interactions and show that, for an engineered two-photon coupling, strong cross-resonant driving can realize a qubit-conditional squeezing operation in a transmon–resonator circuit with an asymmetric SQUID coupler, as supported by numerical simulations with realistic parameters. In trapped ions, Millican et al. [27] use optimal control of modulated Jaynes-Cummings and anti-Jaynes-Cummings interactions to deterministically prepare two-mode squeezed vacuum with up to ~ 6 dB of squeezing.

6.4 | Creation of Controlled-Rotations

The controlled-rotation primitive in Equation (9), can be generated in hybrid qubit–oscillator platforms via a dispersive (number-dependent) interaction of the form

$$H_{\mathrm{disp}} = \frac{\chi}{2}\,\sigma_z\, a^{\dagger} a, \tag{19}$$

which yields a conditional phase-space rotation of angle $\theta = \chi T$ after an idling time T.

In circuit QED, such number-selective conditional phases are routinely implemented and constitute a standard toolbox element (e.g., SNAP-type operations) [58]. In trapped-ion platforms, closely related phonon-number-dependent phase interactions have been proposed within hybrid CV–DV gate toolboxes [68] and are under active experimental development in regimes where strong nonlinearities emerge; see, e.g., recent progress toward nonlinear control outside standard perturbative limits [50].

For broader context on available instruction sets and the experimental status of hybrid qubit–oscillator architectures, see the recent hybrid-processor literature [69, 70].

6.5 | Choosing the Right Code

The bosonic codes we introduced differ by an integer number m defining the number of legs and a positive number r defining the squeezing strength. Beyond this, there exist many other bosonic QECC options [14]. Choosing the right code depends on understanding the dominant noise bias (e.g., loss vs. dephasing), the implementable gate set and calibration complexity (conditional rotations vs. conditional squeezing), and other design factors. Our suggested code has a number-phase structure that offers increasing loss-robustness with larger m while trading resilience to dephasing—precisely the trend quantified in our numeric analysis (Figures 7 and 8). These trade-offs should be optimized for a given platform under its measured loss/dephasing rates.

7 | Summary

We introduced a new family of rotation-symmetric bosonic codes built from coherent superpositions of oriented squeezed vacua. Analytically, the construction yields interleaved Fock-space support $n \equiv 2k \pmod{2m}$ and code distance properties; operationally, a single conditional-squeezing (CS) gate prepares the m=2 instance, while short sequences of conditional rotations extend the scheme to general even m. Using a Knill–Laflamme violation measure, we mapped the trade-off across values of m and benchmarked against cat codes, observing increased loss-robustness with larger m. Finally, we analyzed potential implementations of the squeezed-vacuum codes on existing experimental platforms. These results position the family of squeezed-vacuum codes as a practical number-phase encoding that complements existing cat and binomial families.

Acknowledgments

While working on this paper, we discovered Korolev et al. [71], which beautifully discusses squeezed Fock states as a QECC source, which for n=0 (Vacuum state) is analogous to the m=1 case of our construction [2]. Recently, a work by Hope et al. [72] proposed a scheme for preparing superpositions of orthogonally squeezed states using qubit-oscillator coupling. Their results provide a physical implementation proposal for the $m = 2$ member of the code family analyzed here, further supporting the feasibility of squeezed-vacuum encodings.

This work was supported by the Israel Science Foundation (ISF), Grant No. 385/23 and Grant No. 1315/24. This research project was also partially supported under the Flagship research project QUBIT by the Helen Diller Quantum Center at the Technion.

Conflicts of Interest

The authors declare no conflicts of interest.

Endnotes

[1] colloquially called 'photon-loss,' even though the system may not be photon-based.

[2] or m=2 in the dual-basis.

References

1. P. W. Shor, "Scheme for Reducing Decoherence in Quantum Computer Memory," *Physical Review A* 52, no. 4 (1995): R2493–R2496.

2. D. Gottesman, "Stabilizer Codes and Quantum Error Correction," Ph.D. dissertation, California Institute of Technology (1997).

3. A. Y. Kitaev, "Fault-Tolerant Quantum Computation by Anyons," *Annals of Physics* 303, no. 1 (2003): 2–30.

4. A. G. Fowler, M. Mariantoni, J. M. Martinis, and A. N. Cleland, "Surface Codes: Towards Practical Large-Scale Quantum Computation," *Physical Review A* 86, no. 3 (2012): 032324.

5. D. Horsman, A. G. Fowler, S. Devitt, and R. V. Meter, "Surface Code Quantum Computing by Lattice Surgery," *New Journal of Physics* 14, no. 12 (2012): 123011.

6. M. Reagor, W. Pfaff, C. Axline, et al., "Quantum Memory with Millisecond Coherence in Circuit QED," *Physical Review B* 94 (2016): 014506.

7. O. Milul, B. Guttel, U. Goldblatt, S. Hazanov, L. M. Joshi, D. Chausovsky, N. Kahn, E. Çiftyürek, F. Lafont, and S. Rosenblum, "Superconducting Cavity Qubit with Tens of Milliseconds Single-Photon Coherence Time," *PRX Quantum* 4 (2023): 030336.

8. S. Lloyd and S. L. Braunstein, "Quantum Computation over Continuous Variables," *Physical Review Letters* 82, no. 8 (1999): 1784–1787.

9. I. L. Chuang, D. W. Leung, and Y. Yamamoto, "Bosonic Quantum Codes for Amplitude Damping," *Physical Review A* 56, no. 2 (1997): 1114–1125.

10. P. T. Cochrane, G. J. Milburn, and W. J. Munro, "Macroscopically Distinct Quantum-Superposition States as a Bosonic Code for Amplitude Damping," *Physical Review A* 59, no. 4 (1999): 2631–2634.

11. Z. Leghtas, B. Vlastakis, G. Kirchmair, R. J. Schoelkopf, M. H. Devoret, and M. Mirrahimi, "Hardware-Efficient Autonomous Quantum Memory Protection," *Physical Review Letters* 111, no. 12 (2013): 120501.

12. D. Gottesman, A. Kitaev, and J. Preskill, "Encoding a Qubit in an Oscillator," *Physical Review A* 64, no. 1 (2001): 012310.

13. M. H. Michael, M. P. Silveri, M. Brierley, V. V. Albert, J. Salmilehto, L. Jiang, and S. M. Girvin, "New Class of Quantum Error-Correcting Codes for a Bosonic Mode," *Physical Review X* 6, no. 3 (2016): 031006.

14. V. V. Albert, P. Faist, and many contributors, "The Error Correction Zoo," online resource, https://errorcorrectionzoo.org/ (accessed May 24, 2026).

15. S. L. Braunstein and P. Van Loock, "Quantum Information with Continuous Variables," *Reviews of Modern Physics* 77, no. 2 (2005): 513–577.

16. V. V. Albert, K. Noh, K. Duivenvoorden, D. J. Young, R. T. Brierley, P. Reinhold, C. Vuillot, L. Li, C. Shen, S. M. Girvin, B. M. Terhal, and L. Jiang, "Performance and Structure of Single-Mode Bosonic Codes," *Physical Review A* 97 (2018): 032346.

17. A. L. Grimsmo, J. Combes, and B. Q. Baragiola, "Quantum Computing with Rotation-Symmetric Bosonic Codes," *Physical Review X* 10, no. 1 (2020): 011058.

18. N. Ofek, A. Petrenko, R. Heeres, P. Reinhold, Z. Leghtas, B. Vlastakis, Y. Liu, L. Frunzio, S. M. Girvin, L. Jiang, M. Mirrahimi, M. H. Devoret, and R. J. Schoelkopf, "Extending the Lifetime of a Quantum Bit with Error Correction in Superconducting Circuits," *Nature* 536 (2016): 441–445.

19. L. Hu, Y. Ma, W. Cai, X. Mu, Y. Xu, W. Wang, Y. Wu, H. Wang, Y. P. Song, C.-L. Zou, S. M. Girvin, L.-M. Duan, and L. Sun, "Quantum Error Correction and Universal Gate Set Operation on a Binomial Bosonic Logical Qubit," *Nature Physics* 15 (2019): 503–508.

20. C. Flühmann, V. Nguyen, M. Marinelli, V. Negnevitsky, H. Bekker, Y. Li, and J. P. Home, "Encoding a Qubit in a Trapped-Ion Mechanical Oscillator," *Nature* 566 (2019): 513–517.

21. B. De Neeve, T.-L. Nguyen, T. Behrle, and J. P. Home, "Error Correction of a Logical Grid State Qubit by Dissipative Pumping," *Nature Physics* 18, no. 3 (2022): 296–300.

22. V. V. Sivak, A. Eickbusch, B. Royer, S. Singh, I. Tsioutsios, S. Ganjam, A. Miano, B. L. Brock, A. Z. Ding, L. Frunzio, S. M. Girvin, R. J. Schoelkopf, and M. H. Devoret, "Real-Time Quantum Error Correction Beyond Break-Even," *Nature* 616, no. 7955 (2023): 50–55.

23. M. V. Larsen, J. E. Bourassa, S. Kocsis, J. F. Tasker, R. S. Chadwick, C. González-Arciniegas, J. Hastrup, C. E. Lopetegui-González, F. M. Miatto, A. Motamedi, R. Noro, G. Roeland, R. Baby, H. Chen, P. Contu, I. Di Luch, C. Drago, M. Giesbrecht, T. Grainge, I. Krasnokutska, M. Menotti, B. Morrison, C. Puviraj, K. Rezaei Shad, B. Hussain, J. McMahon, J. E. Ortmann, M. J. Collins, C. Ma, D. S. Phillips, M. Seymour, Q. Y. Tang, B. Yang, Z. Vernon, R. N. Alexander, and D. H. Mahler, "Integrated Photonic Source of Gottesman–Kitaev–Preskill Qubits," *Nature* 642 (2025): 587–591.

24. M. Ayyash, X. Xu, S. Ashhab, and M. Mariantoni, "Driven Multiphoton Qubit-Resonator Interactions," *Physical Review A* 110 (2024): 053711.

25. N. F. Del Grosso, R. G. Cortiñas, P. I. Villar, F. C. Lombardo, and J. P. Paz, "Controlled-Squeeze Gate in Superconducting Quantum Circuits," *Physical Review A* 111, no. 4 (2025): 042606.

26. E. Blumenthal, N. Gutman, I. Kaminer, and S. Hacohen-Gourgy, "Single- and Two-Mode Squeezing by Modulated Coupling to a Rabi-Driven Qubit," *Advanced Quantum Technologies* 9, no. 3 (2026): e00490.

27. M. J. Millican, V. G. Matsos, C. H. Valahu, T. Navickas, L. J. Bond, and T. R. Tan, "Engineering Continuous-Variable Entanglement in Mechanical Oscillators with Optimal Control," *Physical Review Letters* 135, no. 23 (2025): 233604.

28. E. P. Wigner, "On the Quantum Correction for Thermodynamic Equilibrium," *Physical Review* 40 (1932): 749–759.

29. F. Nicacio, R. N. Maia, F. Toscano, and R. O. Vallejos, "Phase Space Structure of Generalized Gaussian Cat States," *Physics Letters A* 374, no. 43 (2010): 4385–4392.

30. D. F. Walls, "Squeezed States of Light," *Nature* 306, no. 5939 (1983): 141–146.

31. Y. Liu, S. Singh, K. C. Smith, E. Crane, J. M. Martyn, A. Eickbusch, A. Schuckert, R. D. Li, J. Sinanan-Singh, M. B. Soley, et al., "Hybrid

Oscillator-Qubit Quantum Processors: Instruction Set Architectures, Abstract Machine Models, and Applications," *PRX Quantum* 7, no. 1 (2026): 010201.

32. A. Kay, "Tutorial on the Quantikz Package," (2023), arXiv:1809.03842 [quant-ph] (2018; version v8, revised 2026), https://doi.org/10.48550/arXiv.1809.03842.

33. "Code," Results in This Paper Are Supported by Our Code, Freely Available on GitHub.

34. Y. Hu, G.-Q. Ge, S. Chen, X.-F. Yang, and Y.-L. Chen, "Cross-Kerr Effect Induced by Coupled Josephson Qubits in Circuit Quantum Electrodynamics," *Physical Review A* 84 (2011): 012329.

35. T. Liu, Y. Zhang, B.-Q. Guo, C.-S. Yu, and W.-N. Zhang, "Circuit QED: Cross-Kerr Effect Induced by a Superconducting Qutrit Without Classical Pulses," *Quantum Information Processing* 16, no. 9 (2017): 209.

36. S. Ding, G. Maslennikov, R. Hablützel, and D. Matsukevich, "Cross-Kerr Nonlinearity for Phonon Counting," *Physical Review Letters* 119 (2017): 193602.

37. R. Raussendorf and H. J. Briegel, "A One-Way Quantum Computer," *Physical Review Letters* 86, no. 22 (2001): 5188–5191.

38. T. Hillmann, F. Quijandría, A. L. Grimsmo, and G. Ferrini, "Performance of Teleportation-Based Error-Correction Circuits for Bosonic Codes With Noisy Measurements," *PRX Quantum* 3, no. 2 (2022): 020334.

39. P. Leviant, Q. Xu, L. Jiang, and S. Rosenblum, "Quantum Capacity and Codes for the Bosonic Loss-Dephasing Channel," *Quantum* 6 (2022): 821.

40. F. A. Mele, F. Salek, V. Giovannetti, and L. Lami, "Quantum Communication on the Bosonic Loss-Dephasing Channel," *Physical Review A* 110 (2024): 012460.

41. E. Knill and R. Laflamme, "Theory of Quantum Error-Correcting Codes," *Physical Review A* 55 (1997): 900–911.

42. P.-O. Löwdin, "On the Non-Orthogonality Problem Connected With the Use of Atomic Wave Functions in the Theory of Molecules and Crystals," *The Journal of Chemical Physics* 18, no. 3 (1950): 365–375.

43. P. Reinhold, "Controlling Error-Correctable Bosonic Qubits," Ph.D. dissertation, Yale University, 2019.

44. G. Zheng, W. He, G. Lee, and L. Jiang, "Near-Optimal Performance of Quantum Error Correction Codes," *Physical Review Letters* 132 (2024): 250602.

45. A. Eickbusch, V. Sivak, A. Z. Ding, S. S. Elder, S. R. Jha, J. Venkatraman, B. Royer, S. M. Girvin, R. J. Schoelkopf, and M. H. Devoret, "Fast Universal Control of an Oscillator With Weak Dispersive Coupling to a Qubit," *Nature Physics* 18 (2022): 1464–1469.

46. H. Liu, V. D. Vaidya, M. Gutierrez Galan, A. K. Ratcliffe, A. Poudel, and C. R. Viteri, "High-Fidelity Raman Spin-Dependent Kicks in the Presence of Micromotion," *Physical Review A* 113 (2026): 043731, https://doi.org/10.1103/972s-wd2q.

47. J. Hastrup, K. Park, J. B. Brask, R. Filip, and U. L. Andersen, "Measurement-Free Preparation of Grid States," *npj Quantum Information* 7, no. 1 (2021): 17.

48. L. P. Gallagher, M. Mazzanti, Z. E. D. Ackerman, R. J. Spreeuw, A. Safavi-Naini, and R. Gerritsma, "Quadratic Spin-Phonon Coupling and Bipolarons in Trapped Ions," *Physical Review A* 112, no. 2 (2025): L020401.

49. M. Stobińska, A. S. Villar, and G. Leuchs, "Generation of Kerr Non-Gaussian Motional States of Trapped Ions," *EPL (Europhysics Letters)* 94, no. 5 (2011): 54002.

50. M. Simoni, I. Rojkov, M. Mazzanti, W. Adamczyk, A. Ferk, P. Hrmo, S. Jain, T. Sägesser, D. Kienzler, and J. Home, "Non-Linear Cooling and Control of a Mechanical Quantum Harmonic Oscillator," *arXiv Preprint arXiv:2509.05734* (2025).

51. C. Kang, M. B. Soley, E. Crane, S. M. Girvin, and N. Wiebe, "Leveraging Hamiltonian Simulation Techniques to Compile Operations on Bosonic Devices," *Journal of Physics A: Mathematical and Theoretical* 58, no. 17 (2025): 175301.

52. L. Guo, T. Huang, and L. Du, "Engineering Bosonic Codes With Quantum Lattice Gates," *Communications Physics* 8, no. 1 (2025): 414.

53. I. Rojkov, M. Simoni, E. Zapusek, F. Reiter, and J. Home, "Stabilization of Cat-State Manifolds Using Nonlinear Reservoir Engineering," *Physical Review X* 16 (2026): 011056, https://doi.org/10.1103/d557-9lr4.

54. Y. Xu, Y. Wang, C. Vuillot, and V. V. Albert, "Letting the Tiger Out of Its Cage: Bosonic Coding Without Concatenation," *Physical Review X* 15, no. 4 (2025): 041025.

55. W. C. Smith, A. Borgognoni, M. Villiers, E. Roverc'h, J. Palomo, M. R. Delbecq, T. Kontos, P. Campagne-Ibarcq, B. Douçot, and Z. Leghtas, "Spectral Signature of High-Order Photon Processes Enhanced by Cooper-Pair Pairing," *Nature Communications* 16, no. 1 (2025): 8359.

56. A. Vanselow, B. Beauseigneur, L. Lattier, M. Villiers, A. Denis, P. Morfin, Z. Leghtas, and P. Campagne-Ibarcq, "Dissipating Quartets of Excitations in a Superconducting Circuit," *Physical Review X* 16 (2026): 011032, https://doi.org/10.1103/bjpc-8xcf.

57. S. Krastanov, V. V. Albert, C. Shen, L. Jiang, S. M. Girvin, and M. Mirrahimi, "Universal Control of an Oscillator With Dispersive Coupling to a Qubit," *Physical Review A* 92 (2015): 040303.

58. R. W. Heeres, B. Vlastakis, E. Holland, S. Krastanov, V. V. Albert, L. Frunzio, L. Jiang, and R. J. Schoelkopf, "Cavity State Manipulation Using Photon-Number Selective Phase Gates," *Physical Review Letters* 115 (2015): 137002.

59. V. Matsos, C. Valahu, T. Navickas, A. Rao, M. Millican, X. Kolesnikow, M. Biercuk, and T. Tan, "Robust and Deterministic Preparation of Bosonic Logical States in a Trapped Ion," *Physical Review Letters* 133, no. 5 (2024): 050602.

60. P. C. Haljan, K.-A. Brickman, L. Deslauriers, P. J. Lee, and C. Monroe, "Spin-Dependent Forces on Trapped Ions for Phase-Stable Quantum Gates and Entangled States of Spin and Motion," *Physical Review Letters* 94 (2005): 153602.

61. M. Drechsler, M. Belén Farías, N. Freitas, C. T. Schmiegelow, and J. P. Paz, "State-Dependent Motional Squeezing of a Trapped Ion: Proposed Method and Applications," *Physical Review A* 101 (2020): 052331.

62. O. Băzăvan, S. Saner, D. Webb, E. M. Ainley, P. Drmota, D. P. Nadlinger, G. Araneda, D. M. Lucas, C. J. Ballance, and R. Srinivas, "Squeezing, Trisqueezing, and Quadsqueezing in a Hybrid Oscillator-spin System," *Nature Physics* 22 (2026): 757–762, https://doi.org/10.1038/s41567-026-03222-6.

63. S. Saner, O. Băzăvan, D. J. Webb, G. Araneda, D. M. Lucas, C. J. Ballance, and R. Srinivas, "Generating Arbitrary Superpositions of Nonclassical Quantum Harmonic Oscillator States," arXiv preprint arXiv:2409.03482 (2024), https://doi.org/10.1103/k1xk-yt42.

64. D. Leibfried, R. Blatt, C. Monroe, and D. Wineland, "Quantum Dynamics of Single Trapped Ions," *Reviews of Modern Physics* 75, no. 1 (2003): 281–324.

65. O. Katz, M. Cetina, and C. Monroe, "N-Body Interactions Between Trapped Ion Qubits via Spin-Dependent Squeezing," *Physical Review Letters* 129 (2022): 063603.

66. Y. Shapira, S. Cohen, N. Akerman, A. Stern, and R. Ozeri, "Robust Two-Qubit Gates for Trapped Ions Using Spin-Dependent Squeezing," *Physical Review Letters* 130 (2023): 030602.

67. O. Katz, L. Feng, A. Risinger, C. Monroe, and M. Cetina, "Demonstration of Three- and Four-Body Interactions Between Trapped-Ion Spins," *Nature Physics* 19 (2023): 1452–1458.

68. R. T. Sutherland and R. Srinivas, "Universal Hybrid Quantum Computing in Trapped Ions," *Physical Review A* 104, no. 3 (2021): 032609.

69. Y. Liu, S. Singh, K. C. Smith, E. Crane, J. M. Martyn, A. Eickbusch, A. Schuckert, R. D. Li, J. Sinanan-Singh, M. B. Soley, et al., "Hybrid Oscillator-Qubit Quantum Processors: Instruction Set Architectures, Abstract Machine Models, and Applications," *PRX Quantum* 7, no. 1 (2026): 010201.

70. J. Y. Araz, M. Grau, J. Montgomery, and F. Ringer, "Hybrid Quantum Simulations With Qubits and Qumodes on Trapped-Ion Platforms," *Physical Review A* 112, no. 1 (2025): 012620.

71. S. B. Korolev, E. N. Bashmakova, and T. Y. Golubeva, "Error Correction Using Squeezed Fock States," *Quantum Information Processing* 23, no. 10 (2024): 354.

72. M. K. Hope, J. Lidal, and F. Massel, "Preparation of Conditionally-Squeezed States in Qubit-Oscillator Systems," arXiv preprint arXiv:2504.01664 (2025).

Supporting Information

Additional supporting information can be found online in the Supporting Information section.

Supporting File: apxr70130-sup-0001-SuppMat.pdf.